Experimental Thermal and Fluid Science 99 (2018) 336–343

Contents lists available at ScienceDirect

Experimental Thermal and Fluid Science

journal homepage: www.elsevier.com/locate/etfs

The influence of microjet array area ratio on heat transfer in the compact heat exchanger

Tomasz Muszynski

Gdansk University of Technology, Faculty of Mechanical Engineering, Department of Energy and Industrial Apparatus, Narutowicza 11/12, 80-233 Gdansk, Poland

ARTICLE INFO

Keywords:
Microjets
Heat exchanger
Heat transfer enhancement
Wilson plot method

ABSTRACT

The paper describes the comprehensive study on the effect of microjet array geometrical parameters on the heat transfer enhancement in the modular heat exchanger. The conducted experimental study provides an experimental database on single phase submerged microjet heat transfer. The Wilson plot method was applied to determine the heat transfer coefficients in the laminar and transition flow regimes of a liquid-to-liquid heat exchanger. The heat exchanger was capable of exchanging 296 W of thermal energy at LMTD of 44 K. The obtained heat transfer coefficient reaches over 24,000 $W/m^2 K$.

Average Nusselt number predictions of the Wen and Jang (2003) correlation were in best agreement with the experimentally determined average Nusselt numbers. In the whole tested flow range, Nusselt numbers were not well correlated by any of the correlations from the literature. The experimentally determined Nusselt numbers were significantly lower than expected, due to limited applicability of given literature correlations.

The author also proposed own experimental correlation for jet impingement heat transfer coefficient, predicting the experimental results within 30%.

1. Introduction

Cost saving strategies and new technologies have led to the design and fabrication of various constructions mini/micro heat exchangers [1–3].

Environmental aspect led to government regulations of emissions of greenhouse gasses reduction. Due to those limitations, renewable energy gains more and more interest in various applications, including the engineering [4], food [5], and agricultural sectors [6]. Nonetheless, significant gains can be made also in these areas by increasing the efficiency of energy utilization, i.e. improving process efficiency [7] or recovering low-grade waste heat. Investments in various industry branches would bring environmental benefits of thousands of tons of carbon dioxide equivalent per year and significant economic advantages due to lower emission fees.

Optimization of energy use, such as improved utilization of existing resources, needs precise data both on the system and its elements characteristics [8]. Demand for defining the waste heat recovery potential in process sites, which would increase energy efficiency, resulted in various well-established methods. Simplified mathematical models are based on waste heat as a primary source for power generation [9], combined cooling and heating [10]. Studies conducted in leading research centers show, that the total energy utilization efficiency can be increased up to 10% with the use of waste heat recovery systems, even 33% if the total recovered heat would be exploited on-site [11].

Efficient heat removal in refrigeration and air-conditioning requires an installation of high-performance heat exchangers i.e. condenser, evaporator or regenerator [12]. Striving to increase the performance of these elements while maintaining the highest possible size to thermal energy ratio is nowadays the main trend in research [13].

As is well known, in recuperators, the heat transfer coefficient has a decisive influence on their efficiency. Many investigators conducted experimental and numerical studies of geometrical parameters on the thermo-hydraulic performance of heat exchangers. Overall heat transfer coefficient is always lower than the lowest heat transfer coefficient from working media. Therefore, a key issue is to enhance the lesser value of heat transfer coefficient. Particularly single phase HTC, which in the case of ORC occurs in transcritical or superheated vapour region [14].

Heat transfer enhancement can be realized by various passive and active techniques. Which are providing means of reducing the thermal resistance of a boundary layer, exploiting various techniques such as nanoparticles [15], surface enhancement [16] louvers [17], longitudinal vortex generators (LVG) [18]. Insertion of swirl flow devices [19] enhances the convective heat transfer by making swirl into the bulk flow and disrupting the boundary layer at the heat transfer surface. As shown in [20], for the LVG were used for heat transfer

E-mail address: Tomasz.Muszynski@pg.edu.pl.

https://doi.org/10.1016/j.expthermflusci.2018.08.010
Received 14 February 2018; Received in revised form 31 July 2018; Accepted 8 August 2018
Available online 09 August 2018

Nomenclature

A	surface of heat transfer [m^2]
A_r	area ratio []
C_0	experimental factor, []
c_p	specific heat, [J/kg K]
d/D	diameter [m]
g	gravitational acceleration [m/s^2]
H	nozzle to impinged surface distance [m]
htc	heat transfer coefficient [W/m^2 K]
k	total heat transfer coefficient [W/m^2 K]
L	channel length [m]
$\dot{m}$	mass flow of fluid, [kg/s]
Nu	Nusselt number []
P_r	Prandtl number []
Re	Reynolds number []
T	temperature [K]
T′	inlet temperature [K]
T″	outlet temperature [K]
U	uncertainty [%]
w	velocity [m/s]
$\dot{Q}$	heat flow [W]

Greek symbols

δ	thickness of membrane [m]
λ	thermal conductivity [W/m K]
μ	dynamic viscosity [Pas]
ν	kinematic viscosity [m^2/s]

Superscripts

air	air
c	cold
eq	equation
exp	experimental
h	hot
w	wall

augmentation. Results demonstrate that the field synergy principle reveals the inherent mechanism of heat transfer enhancement with LVG.

Methods to intensify the heat transfer by means of jet cooling was presented in the work of Martin [21], who analyzed different impinging gas jets. His research focused on involving the nozzle geometry and a number of jets (single or arrays) with heat transfer coefficient. Also, key geometric nozzle parameters (round, or slot) for the different configurations were taken into the account. A lot of interest regarding microjet cooling especially in electronics resulted in a development of jet impingement correlations such as one by Li and Garimella [22]. Authors focused on finding the influence of Prandtl number on the local and average heat transfer coefficient during jet impingement. Experiments were conducted on three different liquids and air with varying Reynolds number, nozzle diameters, and nozzle to plate distance. The area-weighted average of the impingement region and the wall jet region heat transfer coefficients were used to describe average Nusselt numbers.

In the review by Meola [23] a new correlation for the average Nusselt number based on the database available in the literature was proposed. New formula attempts to include effects of jet forming nozzle on heat transfer for an array of jets impinging on a flat surface.

An experimental study by Vinze et al. [24] was carried out to investigate the local heat transfer distribution for impinging jets. Authors also studied nozzle chevron effect on heat transfer. Similar numerical study on the effect of the nozzle shape on heat transfer was presented by Marzec and Kucaba [25]. The cylindrical, convergent and divergent geometry of the nozzles were taken into consideration. The results indicated that cylindrical geometry of the nozzles results in the highest Nusselt numbers along the cooled surface.

Microjet heat transfer enhancement besides use in high-performance applications (such as LED arrays cooling) was also used in micro heat exchangers was also investigated [26]. The overall heat transfer coefficients presented for a single phase water forced convection, reaches over 10 kW/m^2 K. Obtained results for a heat exchanger geometry indicated that significant heat transfer enhancement can be obtained with low pumping power requirements. With potential significant gains due to the micronozzle geometry optimization [27].

The jet enhancement was successfully adopted for the innovative construction of a forced air solar heater. Based on a confined single slot jet of air impinging on the flat surface of a solar absorber plate. A comparison of the experimental results of thermal-flow performance of different types of air solar heaters indicated that the tested device can compete with the best commercially available solutions. It was found that the single glass covering significantly improves the efficiency of solar energy conversion from 16% up to 24%. Also, the pressure losses associated with air passing through the developed device were the lower than in compared solar air heaters [28].

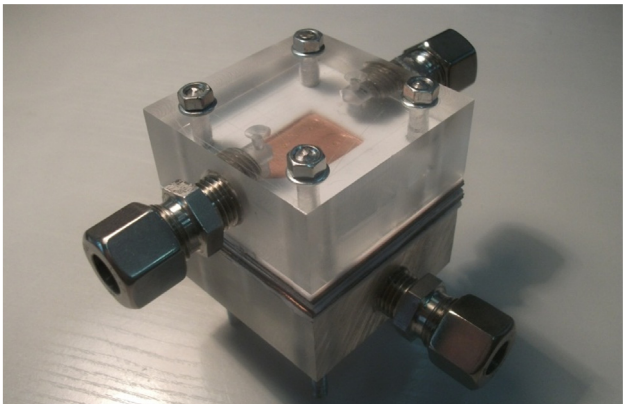

Fig. 1. View on microjet heat exchanger.

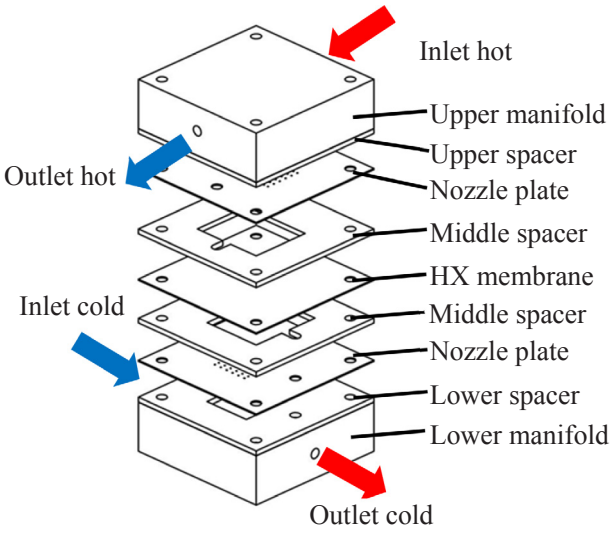

Fig. 2. Schematic of modular microjet heat exchanger.

Different solar air heater construction with jet technology was pursued by Rajaseenivasan et al. [29]. Their study concentrated on the

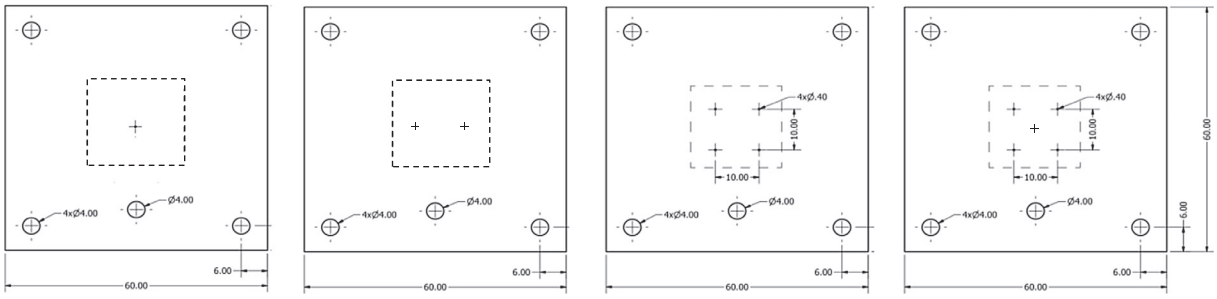

Fig. 3. Schematics of microjet nozzle plates used during experiments.

Table 1
Heat exchanger design parameters.

Parameter	Value	Unit	Uncertainty
Heat transfer area	400	[mm^2]	± 2.8
No. of jets	1–5	[–]	
Jets nozzle diameter	0.6	[mm]	± 0.01
Jet standoff	2	[mm]	± 0.05
Inlet temperatures	10–80	[°C]	± 0.1
Fluid flow rate	0.028–0.138	[kg/s]	± 0.0005
Pressure drop	1.5–40	[kPa]	± 0.075%
Operating pressure	200	[kPa]	± 0.15

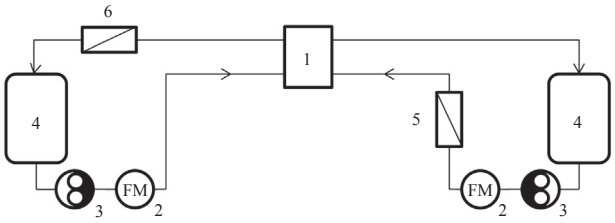

Fig. 4. Schematic view of a test facility loop: 1 – modular heat exchanger, 2 – mass flow meter, 3 – micro gear pump, 4 – fluid supply vessel, 5 – heat exchanger connected with ultra-thermostat, 6 – heat exchanger connected with chiller.

Table 2
Experimental uncertainty.

Variable	Uncertainty (%)
ΔT	1.1–1.6%
v_{jet}	16–16.7%
q	6.8–7.4%
k	8–10.8%
Re	8.3%

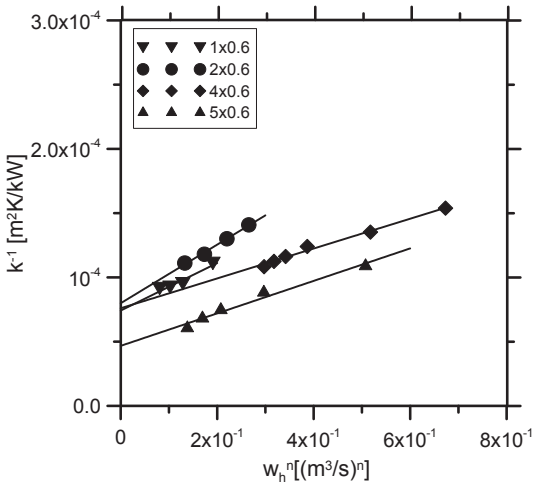

Fig. 6. Sample scheme for calculating the heat transfer coefficient by Wilsons plot method, for various geometries.

effect of varying angles of attack on the heat transfer rate. The proposed solar air heater is compared with the performance of conventional solar air heater. The maximum thermal enhancement factor of 2.19 was achieved with the mass flow rate of 0.016 kg/s, a nozzle diameter of 5 mm and 30° angle of attack.

Karwa et al. [30] presented experimental investigations on a submerged multi-jet impingement heat sink. The research was performed on 3D printed prototype microjet heat sink with microjet technology, with the aim to obtain a lowest thermal resistance, which for the proposed design was 0.025 K/W at the pressure drop of 25 kPa.

As can be seen in the literature review there is a universal need to develop compact, efficient heat exchangers in order to rise up to both economic and technical challenges of energy systems. Unfortunately, there is a need for a better understanding of the impact of fluid-wall flow schemes on the thermal performance of mini/micro heat

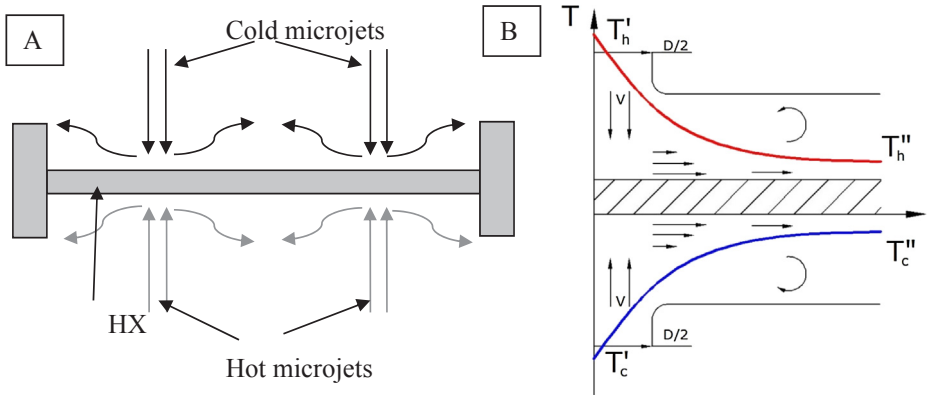

Fig. 5. (A) The possible flow pattern in the tested heat exchanger, (B) Flow pattern and temperature distribution of impinging jet.

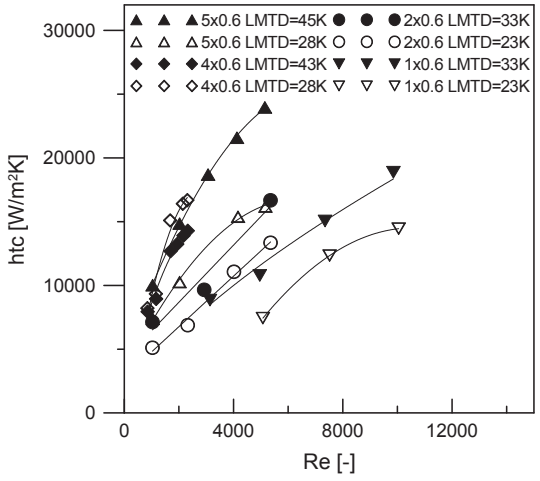

Fig. 7. Experimentally obtained heat transfer coefficient values.

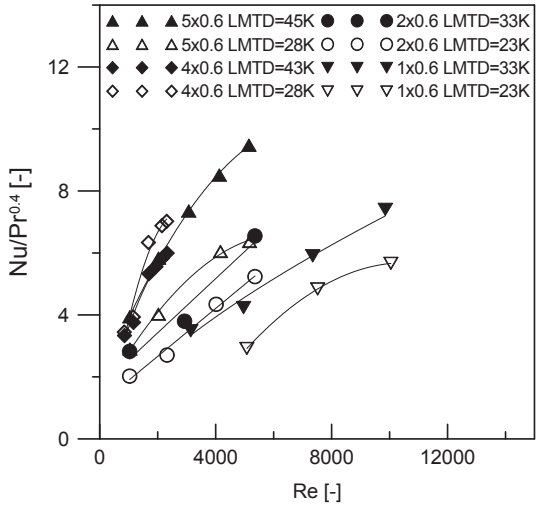

Fig. 8. Experimental values of Nusselt to Prandtl ratio in function of Reynolds number.

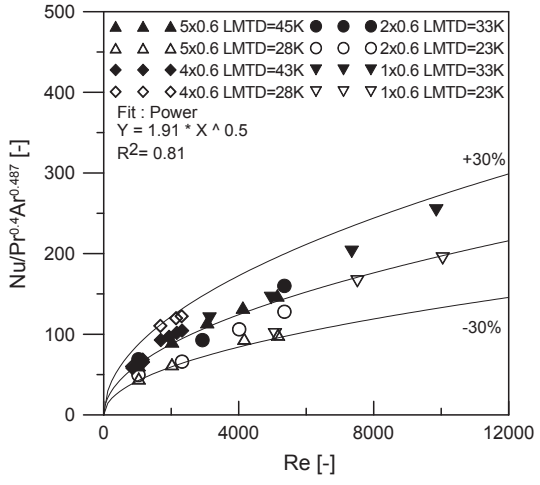

Fig. 9. Evaluation of area ratio influence on experimental data.

exchangers is still needed for the development of highly efficient equipment.

This paper describes the comprehensive study on the effect of microjet array geometrical parameters on the heat transfer enhancement

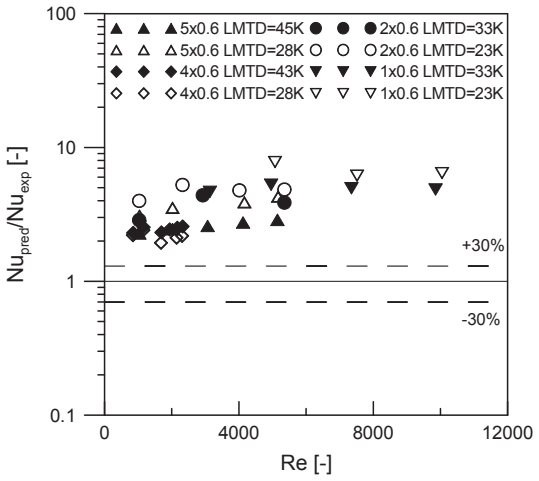

Fig. 10. Comparison between predicted by Li and Garimella [22] and experimental average Nusselt numbers.

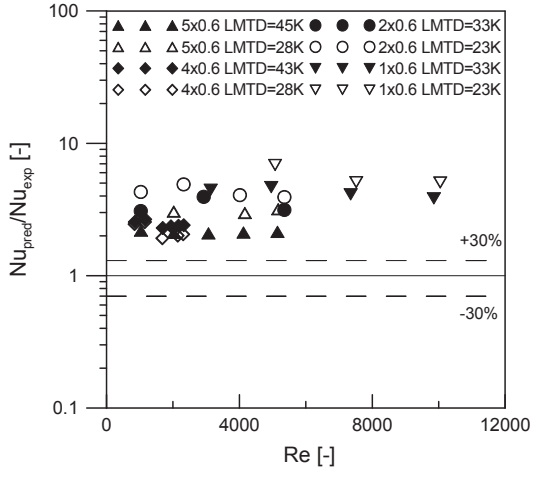

Fig. 11. Comparison between predicted by Lytle and Web [41] and experimental average Nusselt numbers.

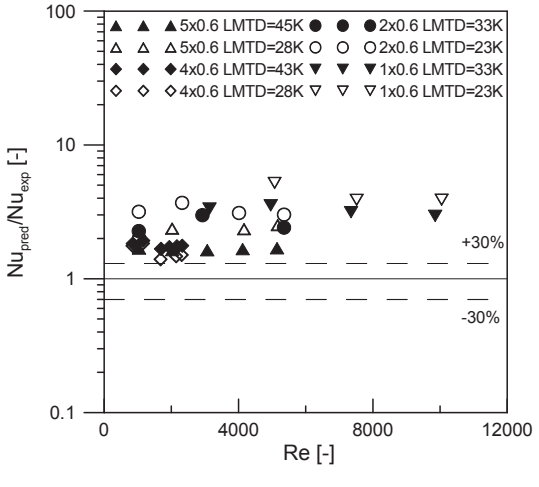

Fig. 12. Comparison between predicted by Michna [37] and experimental average Nusselt numbers.

in the modular heat exchanger. The heat exchanger is based on jet impingement on the flat heat transfer surface. It comprises two symmetrical flow arrangements for two fluids. The modular design of the heat exchanger was presented in the author's previous research [31].

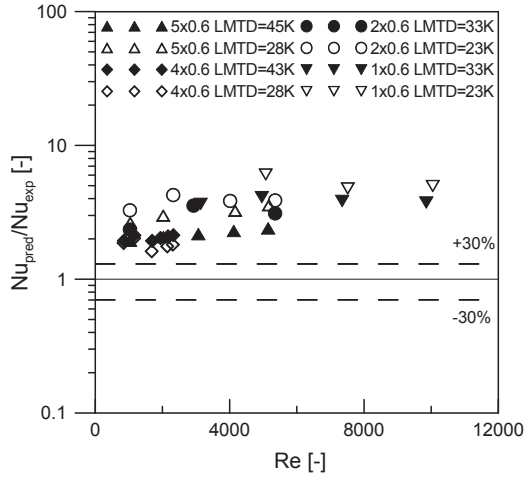

Fig. 13. Comparison between predicted by Meola [23] and experimental average Nusselt numbers.

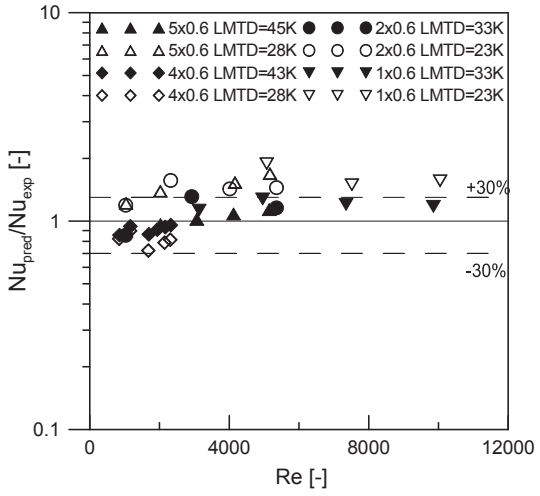

Fig. 14. Comparison between predicted by Wen and Jang [40] and experimental average Nusselt numbers.

The primary objectives of the present study are to:

(1) Provide an experimental database on single phase submerged microjet heat transfer
(2) Recognize the effect of nozzle array dimensions on heat transfer
(3) Conduct a systematic assessment of predictive techniques

2. Experimental test setup

2.1. Modular heat exchanger design

Investigated is the microjet heat exchanger, recuperator type. It's comprised of a series of plates. Impinging jets are created by introducing 1 mm thick laminate plates with nozzles. The nozzles were created by drilling. These plates are separated by spacers/gaskets made of Polytetrafluoroethylene – PTFE. Microjet geometry can be varied by exchanging the nozzle plates and spacers of the heat exchanger. Heat exchange between the working fluids is performed through 1 mm thick plate made of the aluminum alloy EN AW-1050A, with a heat exchange surface 4 cm^2. Structural details and a description of the exchanger are shown in Figs. 1 and 2.

Fig. 2 presents the heat exchanger exploded view. Because during the screwing the compression of spacers and membranes may cause some distortion in the collector (made with Polymethyl methacrylate - PMMA) to prevent leakage between its plates, thin seal with high-temperature silicone compound was applied.

In this work, the experimental data for four geometries with varying nozzle spacing were gathered. Fig. 3 presents the view on microjet nozzle plates used during the experiments. In all cases, the 0.6 mm diameter nozzle was created, resulting in the nozzle to wetted area ratio of 7×10^{-4} to 3.5×10^{-3}. In all cases, the height of the nozzle above the heat exchanging membrane was 2 mm. All of the heat exchangers design and operating parameters are listed in Table 1.

2.2. Experimental rig design

The present research demonstrates the results of steady-state heat transfer experiments, carried out for single-phase heat transfer. Data are gathered in steady-state conditions in order to obtain operating temperatures of working fluids and heat flux from energy balance. Steady state operation allows excluding the heat capacity of the heat exchanger casing. The amount of heat transferred is determined during each measurement point. Test facility consisted of a heat exchanger, a fluid supply system, measuring devices, an ultra-thermostatic bath and a refrigerating chiller unit. In both cold and hot fluid circuit, fluid was fed by a magnetically driven micro gear pump from the supply vessel. The desired fluid flow rate was achieved by means of an inverter and a regulation valve. The flow rate was determined using a Coriolis mass flow meter. The total power of the heat exchanger was calculated based on the mass and energy balance. Measurements took place in steady state conditions.

T-type thermocouples (pre-calibrated using a dry box temperature

Table 3
Selected literature impinging jets heat transfer correlations.

Source	Correlation	Exp. range
Li and Garimella [22]	$\overline{Nu} = 0.160 Re_D^{0.695} Pr^{0.4} \left(\frac{h}{D}\right)^{-0.11} \left(\frac{d}{D}\right)^{-0.11}$	$4000 \leqslant ReD \leqslant 23,000$ $1,59 \leqslant D \leqslant 12,5$ mm $1 \leqslant H/D \leqslant 5$, air, water, FC77
Wen and Jang [40]	$\overline{Nu} = 0.442 Re_D^{0.696} Pr^{1/3} \left(\frac{h}{D}\right)^{-0.20} \left(\frac{d/2}{D}\right)^{-0.41}$	$500 \leqslant Re_D \leqslant 27,000$ $3 \leqslant H/D \leqslant 16$, air
Lytle and Web [41]	$\overline{Nu} = 0.726 Re_D^{0.53} \left(\frac{h}{D}\right)^{-0.191}$	$3600 \leqslant Re_D \leqslant 27,600$ $0.1 \leqslant H/D \leqslant 10$, air
Meola [23]	$\overline{Nu} = 0.3 Re_D^{0.68} C_F^{0.56} \left(\frac{D}{H}\right)^{0.3} A_r^{0.15} Pr^{0.42}$	$250 \leqslant Re_D \leqslant 98,000$ $0.39 \leqslant D \leqslant 50$ mm, air, water
Michna [37]	$\overline{Nu} = 0.675 Re_D^{0.55} Pr^{0.243} \cos(5.416Ar - 1.259)$	$50 \leqslant Re_D \leqslant 5100$ D = 54, 112 μm air, water

calibrator) were used to measure the temperature at the inlets and outlets of the heat exchanger. The signal from the thermocouples was acquired with National Instruments collection kit and was processed using the application in the LabVIEW environment. The heat was supplied by a constant temperature bath in the hot water circuit. The total input power is determined by measuring the fluid flow rate and its temperature increase. During the tests, the heat exchanger was able to dissipate up to 293 W for the 5 × 0.6 mm nozzle configuration. The whole set was thermally insulated.

The source of heat is a laboratory grade ultra-thermostat with the heating power of 2 kW, and temperature stability of ± 0.05 °C. Cold water circulates in the second cycle with heat rejection controlled by means of a refrigeration chiller unit. The whole set allows obtaining a long-term constant temperature at the inlets of the heat exchanger. The diagram of the test loop is shown in Fig. 4.

Pressure drop measurement was carried out at the cold water circuit using the piezoelectric smart differential pressure transmitter, with a measuring range of 5–500 kPa, and the measuring accuracy is ± 0.065%FS. The pressure at the inlet and outlet of the heat exchanger is also controlled using absolute pressure transducers (measurement is therefore duplicated). The temperature at the inlets and outlets of the heat exchanger was measured by means of thermocouples T in 1st class. The thermal and flow measurements of the following parameters were recorded: the hot fluid temperature at the inlet (T_h') and outlet (T_h'') of the exchanger, the temperature of the cold fluid at the inlet (T_c') and outlet (T_c'') of the exchanger, and volumetric flow rate of the two fluids. The pressure at the inlet (P_h' and P_c') and the outlet of the heat exchanger (P_h'' and P_c'').

2.3. Measurements uncertainty

In order to determine the reliability of the experimental results, an uncertainty analysis was conducted on all measured quantities. Table 1 shows all of the heat exchanger design and operating parameters, along with measurement uncertainty. The uncertainties of crucial parameters were estimated according to the standard procedures described by NIST [32]. For obtaining the heat transfer coefficients the graphical Wilson plot method is used. Its accuracy depends on the experimental data fit, for all cases the R^2 fit parameter was higher than 0.98. Overall, the uncertainty in the calculated total heat transfer coefficient k is lower than 11% for all experiments. Uncertainties of the other calculated variables are shown in Table 2. For all geometrical configurations, two experimental series were carried out for varying hot fluid inlet temperature, while the cold fluid inlet temperature was kept at a constant level of 9 °C.

The heat losses through convection and radiation to the surroundings were calculated based on the casing temperature and accounted for in all experimental points. Airside heat transfer coefficient was determined for the case of natural convection, according to the procedure described in the author's previous study [31]. In all test cases, the heat loss was not exceeding 5% of the transferred heat rate.

3. Data reduction and results

Experimental setup allows gathering data regarding convective heat transfer between two working fluids. Transferred heat can be calculated based on the temperature rise of flowing liquid for both hot and cold side as written in Eqs. (1) and (2).

$$\dot{Q}_c = \dot{m}_c c_{pc} \Delta T_c \tag{1}$$

$$\dot{Q}_h = \dot{m}_h c_{ph} \Delta T_h \tag{2}$$

Obtained heat flux, is then used to calculate total heat transfer coefficient from Eq. (3).

$$\dot{Q} = kA\Delta T \tag{3}$$

Due to minor loses heat flux values calculated by Eqs. (1) and (2) differ. Difference typically is less than 2%. For further calculations heat absorbed by cold medium Eq. (1) was taken into account.

Heat exchanger geometry indicates that the microjets are fully submerged. The flow arrangement can be depicted as presented in Fig. 5. Fluid microjets impinge the heat exchangers membrane from both sides. Thus heat transfer area is, in fact, the wetted surface of membrane i.e. 4 cm^2. Flow arrangement is rather complicated, but if the wall jet region is to be taken into account, it has obviously a co-current pattern (Fig. 5B). After assuming constant heat flux on the heat exchange surface, thus logarithmic mean temperature difference (LMTD) can be used:

$$\Delta T = \frac{(T_h' - T_c') - (T_h'' - T_c'')}{\ln\left(\frac{(T_h' - T_c')}{(T_h'' - T_c'')}\right)} \tag{4}$$

For calculating heat transfer coefficient (HTC) in the heat exchanger a graphical Wilsons plot method [33]. The method is widely used for various heat exchanger constructions [34–36]. Allows calculating HTC of given working fluid, based on total heat transfer in heat exchanger *(k)* for varying fluid flow rate. The detailed description of the method can be found in studies mentioned previously, therefore this part is omitted.

3.1. Experimental results

The heat exchanger was capable of exchanging up to 293 W of heat at LMTD of 44 K.

Fig. 6 presents sample linear regression values of experimental data series for calculating HTC with Wilsons plot method, for constant cold fluid velocity, and constant supply temperature. The n parameter to which flow rate is raised was equal to 0.8, based on experimental fit. As can be seen, the nozzle geometry has a significant effect on the heat transfer coefficient. The heat transfer coefficient calculations by Wilson's method were conducted for the plate thickness of 1 mm, where the plate material (the aluminum alloy) has the thermal conductivity λ equal to 207 W/m K.

Experimental data were collected for hot water supply at two constant temperature levels i.e. 45 and 62. The dimensional heat transfer performance of the arrays is shown in Fig. 7. Because inlet fluid parameters and the nozzle diameter is assumed as characteristic length and fluid properties in Reynolds number, thus despite constant flow rate Reynolds numbers can vary significantly with hot water supply temperature. Heat transfer coefficients up to 24 kW/m^2 K were obtained using geometry with five microjets. As been expected the geometry with single microjet obtained much lower heat transfer coefficients, due to lower area ratio and lower influence of stagnation point peak heat transfer.

A dimensional analysis of the geometric and fluid parameter relevant to the heat transfer performance of arrays of circular microjets suggests that the Nusselt number has a functional dependence [37] as shown in the following equation:

$$Nu = f(Re; Pr; Ar) \tag{5}$$

In this paper, the experiments include the heat transfer performance over a large range of Reynolds numbers using deionized water as the working fluid. Based on data shown in Table 1, the microjet arrays had five different area ratios in the range $0.0007 < Ar < 0.0035$. Experimentally obtained values of area-averaged heat transfer coefficients are presented in Fig. 7. As expected, the performance of various heat exchanger geometries was clearly dependent on the Reynolds number and temperature. In all array configurations, the heat transfer increased monotonically with Reynolds number.

The standoff distance (the distance between the jet exit and the heat exchanging membrane) was constant and equal to 2 mm for the studied device. Consequently, the all of the tested geometries with 600 μm-

diameter orifices had the same standoff ratio H/D. The dimensionless Nusselt number was calculated based on nozzle diameter as a characteristic dimension:

$$Nu = \frac{htc \cdot D}{\lambda} \tag{6}$$

Due to the fact that the experiments were performed for varying water supply temperature, the influence of the Prandtl number can be observed. Therefore obtained heat transfer data was also presented in form of dimensionless Nusselt to Prandtl ratio, in Fig. 8. As can be seen, obtained data still presents a lot of scattering, and evidently, the influence of temperature difference is visible despite taking Prandtl number into account.

The experimental data from all four microjet geometries was fit with a least squares method to the parameters presented in eq.(5), resulting in:

$$Nu = 1.91 \cdot Re^{0.5} \cdot Pr^{0.4} Ar^{0.487} \tag{7}$$

As can be seen in Fig. 9, the heat transfer performance is captured quite well by this equation. The area-averaged Nusselt numbers calculated from eq. (7) were within ± 30% of the measured value also over 75% of the data points were predicted within ± 20% error band.

The dependence on the Reynolds number is typical of what has been previously reported for arrays of jets. The exponent of 0.5 is the same as used in the correlation of Womac et al. [38] in the “impingement zone”, and similar to Michna et al. [37] study.

Because of the limited Prandtl number variance, its exponent value was also based on other experimental studies. However, future work by the author will investigate the performance of these geometries with refrigerants, which will provide additional information on the Prandtl number dependence.

It is possible that the change of the temperature affects viscosity in the wall jet region, which affects heat transfer. Usually for flows with the large core to wall temperature differences Sieder and Tate [39] approach to include fluids wall to core viscosity ratio. Unfortunately, in the presented experimental scheme, the temperature is measured at the inlet and outlet of the heat exchanger, in which case the hotter wall fluid can be mixed with the colder secondary flow. Regarding the geometric parameters, more data obtained over a wider range of area ratios should be obtained to verify the functional form of the area ratio dependence.

3.2. Comparison with literature

Values of heat transfer coefficient are crucial in energy and process apparatus design. In order to estimate the use of experimental correlations to build heat exchangers with microjet enhancement, experimental results were compared to known literature correlations for impinging jets heat transfer. The heat transfer coefficient depends on many factors, which are usually grouped into two main groups, namely fluid properties and geometric characteristics. The fluid properties describe its thermal and dynamic characteristics. Usually, they are expressed with the Prandtl, *Pr*, and the Reynolds, *Re*, numbers. In the geometric characteristics group generally, the dimensionless quantities *H/D,* and *d/D* are considered. In general, the nozzle diameter is assumed as the characteristic length in Nusselt and Reynolds numbers.

Direct comparison of experimentally obtained values of HTC in form of dimensionless Nusselt numbers is presented in Figs. 10–14.

A very large divergence between prediction given in literature and experiment is visible. We need to note that the selected literature correlations in Table 3 are developed for the average heat transfer rate on the test surface for particular experimental setup and flow parameters. As can be clearly seen experimentally obtained values of heat transfer are in most cases much lower than predictions. The difference may be attributed to the different setup of outlet manifold in the tested heat exchanger, thus different flow pattern than in specified test facilities. Which indicates that flow arrangement has a significant influence on obtained results, and that given correlations are limited in validity to specific working fluids and ranges of operating parameters for the data upon which these models are based.

The best consistency is obtained for Wen and Jang [40] correlation, which predicts 75% of the data within ± 30% error. With the maximum deviation from predictions up to 69%. The correlation by Michna [37] offered predictions higher than experimental values from +39% to 400%. The correlations by Li and Garimella [22], Lytle and Web [41] and Meola [23] over predicted all of the data by as much as six times.

4. Conclusions

The paper describes the comprehensive study on the effect of microjet array geometrical parameters on the heat transfer enhancement in the modular heat exchanger. The heat exchanger is based on jet impingement on the flat heat transfer surface. It comprises two symmetrical flow arrangements for two fluids. The conducted experimental study provides an experimental database on single phase submerged microjet heat transfer.

The Wilson plot method was successfully applied to determine the heat transfer coefficients in the laminar and transition flow regimes of a liquid-to-liquid heat exchanger. The heat exchanger is capable of exchanging 296 W of thermal energy at LMTD of 44 K. The obtained heat transfer coefficient reaches over 24,000 $W/m^2 K$.

Average Nusselt number predictions of the Wen and Jang [40] correlation were in best agreement with the experimentally determined average Nusselt numbers. Better correlation of the data was produced by Eq. (7). In the whole tested flow range, Nusselt numbers were not well correlated by any of the correlations from the literature. The experimentally determined Nusselt numbers were significantly lower than expected, due to limited applicability of given literature correlations. The new correlation was suggested, predicting the experimental results within 30% error.

The heat transfer enhancement in the tested heat exchanger will be further pursuit in the optimization with respect to the spacing and quantity of nozzles to reduce the pressure drop and increase heat transfer rates.

Acknowledgments

The work presented in the paper was partially funded by statuary activity of faculty of Mechanical Engineering of Gdansk University of Technology.

References

[1] Y. Zhao, Y. Liang, Y. Sun, J. Chen, Development of a mini-channel evaporator model using R1234yf as working fluid, Int. J. Refrig. 35 (2012) 2166–2178, https://doi.org/10.1016/j.ijrefrig.2012.08.026.
[2] T. Muszynski, Design and experimental investigations of a cylindrical microjet heat exchanger for waste heat recovery systems, Appl. Therm. Eng. 115 (2017) 782–792, https://doi.org/10.1016/j.applthermaleng.2017.01.021.
[3] K. Guo, N. Zhang, R. Smith, Optimisation of fin selection and thermal design of counter-current plate-fin heat exchangers, Appl. Therm. Eng. 78 (2015) 491–499, https://doi.org/10.1016/j.applthermaleng.2014.11.071.
[4] T.L. Oliveira, P.S. Assis, E.M. Leal, J.R. Ilídio, Study of biomass applied to a co-generation system: A steelmaking industry case, Appl. Therm. Eng. 80 (2015) 269–278, https://doi.org/10.1016/j.applthermaleng.2015.01.002.
[5] J. Ebner, C. Babbitt, M. Winer, B. Hilton, A. Williamson, Life cycle greenhouse gas (GHG) impacts of a novel process for converting food waste to ethanol and co-products, Appl. Energy. 130 (2014) 86–93, https://doi.org/10.1016/j.apenergy.2014.04.099.
[6] P. Olszewski, Heat recovery investigation from dryer–thermal oxidizer system in corn-ethanol plants, Appl. Therm. Eng. 81 (2015) 210–222, https://doi.org/10.1016/j.applthermaleng.2015.02.033.
[7] P. Ostrowski, M. Pronobis, L. Remiorz, Mine emissions reduction installations, Appl. Therm. Eng. 84 (2015) 390–398, https://doi.org/10.1016/j.applthermaleng.2015.03.061.
[8] R. Andrzejczyk, T. Muszynski, C.A. Dorao, Experimental investigations on adiabatic frictional pressure drops of R134a during flow in 5 mm diameter channel, Exp.

Therm. Fluid Sci. 83 (2017) 78–87, https://doi.org/10.1016/j.expthermflusci.2016.12.016.
[9] B. Peris, J. Navarro-Esbrí, F. Molés, R. Collado, A. Mota-Babiloni, Performance evaluation of an Organic Rankine Cycle (ORC) for power applications from low grade heat sources, Appl. Therm. Eng. 75 (2015) 763–769, https://doi.org/10.1016/j.applthermaleng.2014.10.034.
[10] W. Stanek, W. Gazda, W. Kostowski, Thermo-ecological assessment of CCHP (combined cold-heat-and-power) plant supported with renewable energy, Energy. 92 (2015) 279–289, https://doi.org/10.1016/j.energy.2015.02.005.
[11] G. Oluleye, M. Jobson, R. Smith, S.J. Perry, Evaluating the potential of process sites for waste heat recovery, Appl. Energy. 161 (2016) 627–646, https://doi.org/10.1016/j.apenergy.2015.07.011.
[12] J. Sun, W. Li, Operation optimization of an organic rankine cycle (ORC) heat recovery power plant, Appl. Therm. Eng. 31 (2011) 2032–2041, https://doi.org/10.1016/j.applthermaleng.2011.03.012.
[13] N. Tran, Y. Chang, J. Teng, R. Greif, Enhancement heat transfer rate per unit volume of microchannel heat exchanger by using a novel multi-nozzle structure on cool side, Int. J. Heat Mass Transf. 109 (2017) 1031–1043, https://doi.org/10.1016/j.ijheatmasstransfer.2017.02.058.
[14] X. Wang, Y. Dai, Exergoeconomic analysis of utilizing the transcritical CO2 cycle and the ORC for a recompression supercritical CO2 cycle waste heat recovery: A comparative study, Appl. Energy. 170 (2016) 193–207, https://doi.org/10.1016/j.apenergy.2016.02.112.
[15] M. Sheikholeslami, M.K. Sadoughi, Simulation of CuO-water nanofluid heat transfer enhancement in presence of melting surface, Int. J. Heat Mass Transf. 116 (2018) 909–919, https://doi.org/10.1016/J.IJHEATMASSTRANSFER.2017.09.086.
[16] R. Andrzejczyk, T. Muszynski, Performance analyses of helical coil heat exchangers. The effect of external coil surface modification on heat exchanger effectiveness, Arch. Thermodyn. 37 (2016) 137–159, https://doi.org/10.1515/aoter-2016-0032.
[17] T. Muszynski, S.M. Koziel, Parametric study of fluid flow and heat transfer over louvered fins of air heat pump evaporator, Arch. Thermodyn. 37 (2016) 45–62, https://doi.org/10.1515/aoter-2016-0019.
[18] J.M. Wu, H. Zhang, C.H. Yan, Y. Wang, Experimental study on the performance of a novel fin-tube air heat exchanger with punched longitudinal vortex generator, Energy Convers. Manag. 57 (2012) 42–48, https://doi.org/10.1016/J.ENCONMAN.2011.12.009.
[19] M. Sheikholeslami, M. Gorji-Bandpy, D.D. Ganji, Review of heat transfer enhancement methods: focus on passive methods using swirl flow devices, Renew. Sustain. Energy Rev. 49 (2015) 444–469.
[20] J.M. Wu, W.Q. Tao, Investigation on laminar convection heat transfer in fin-and-tube heat exchanger in aligned arrangement with longitudinal vortex generator from the viewpoint of field synergy principle, Appl. Therm. Eng. 27 (2007) 2609–2617, https://doi.org/10.1016/J.APPLTHERMALENG.2007.01.025.
[21] H. Martin, Heat and Mass Transfer between Impinging Gas Jets and Solid Surfaces, Adv. Heat Transf. 13 (1977) 1–60, https://doi.org/10.1016/S0065-2717(08)70221-1.
[22] C.Y. Li, S.V. Garimella, Prandtl-number effects and generalized correlations for confined and submerged jet impingement, Int. J. Heat Mass Transf. 44 (2001) 3471–3480, https://doi.org/10.1016/S0017-9310(01)00003-5.
[23] C. Meola, A New Correlation of Nusselt Number for Impinging Jets, Heat Transf. Eng. 30 (2009) 221–228, https://doi.org/10.1080/01457630802304311.
[24] R. Vinze, S. Chandel, M.D. Limaye, S.V. Prabhu, Local heat transfer distribution between smooth flat surface and impinging incompressible air jet from a chevron nozzle, Exp. Therm. Fluid Sci. 78 (2016) 124–136, https://doi.org/10.1016/j.expthermflusci.2016.05.017.
[25] K. Marzec, A. Kucaba-Pietal, Numerical investigation of local heat transfer distribution on surfaces with a non-uniform temperature under an array of impinging jets with various nozzle shapes, J. Theor. Appl. Mech. 55 (2017) 1313–1324, https://doi.org/10.15632/jtam-pl.55.4.1313.
[26] T. Muszynski, R. Andrzejczyk, Applicability of arrays of microjet heat transfer correlations to design compact heat exchangers, Appl. Therm. Eng. 100 (2016) 105–113, https://doi.org/10.1016/j.applthermaleng.2016.01.120.
[27] T. Muszynski, D. Mikielewicz, Structural optimization of microjet array cooling system, Appl. Therm. Eng. 123 (2017) 103–110, https://doi.org/10.1016/j.applthermaleng.2017.05.082.
[28] M. Zukowski, Experimental investigations of thermal and flow characteristics of a novel microjet air solar heater, Appl. Energy. 142 (2015) 10–20, https://doi.org/10.1016/j.apenergy.2014.12.052.
[29] T. Rajaseenivasan, S. Ravi Prasanth, M. Salamon Antony, K. Srithar, Experimental investigation on the performance of an impinging jet solar air heater, Alexandria Eng. J. 56 (2017) 63–69, https://doi.org/10.1016/j.aej.2016.09.004.
[30] N. Karwa, C. Stanley, H. Intwala, G. Rosengarten, Development of a low thermal resistance water jet cooled heat sink for thermoelectric refrigerators, Appl. Therm. Eng. (2016), https://doi.org/10.1016/j.applthermaleng.2016.06.118.
[31] T. Muszynski, R. Andrzejczyk, Heat transfer characteristics of hybrid microjet - Microchannel cooling module, Appl. Therm. Eng. 93 (2016) 1360–1366, https://doi.org/10.1016/j.applthermaleng.2015.08.085.
[32] B.N. Taylor, C.E. Kuyatt, Guidelines for Evaluating and Expressing the Uncertainty of NIST Measurement Results, NIST Tech. Note. 1297 (1994) 20, https://doi.org/10.6028/NIST.TN.1900.
[33] J.W. Rose, Heat-transfer coefficients, Wilson plots and accuracy of thermal measurements, Exp. Therm. Fluid Sci. 28 (2004) 77–86, https://doi.org/10.1016/S0894-1777(03)00025-6.
[34] P. Fernando, B. Palm, T. Ameel, P. Lundqvist, E. Granryd, A minichannel aluminium tube heat exchanger - Part I: Evaluation of single-phase heat transfer coefficients by the Wilson plot method, Int. J. Refrig. 31 (2008) 669–680, https://doi.org/10.1016/j.ijrefrig.2008.02.011.
[35] X. Lu, X. Du, M. Zeng, S. Zhang, Q. Wang, Shell-side thermal-hydraulic performances of multilayer spiral-wound heat exchangers under different wall thermal boundary conditions, Appl. Therm. Eng. 70 (2014) 1216–1227, https://doi.org/10.1016/j.applthermaleng.2014.02.053.
[36] N. Jamshidi, M. Farhadi, D.D. Ganji, K. Sedighi, Experimental analysis of heat transfer enhancement in shell and helical tube heat exchangers, Appl. Therm. Eng. 51 (2013) 644–652, https://doi.org/10.1016/j.applthermaleng.2012.10.008.
[37] G.J. Michna, E.A. Browne, Y. Peles, M.K. Jensen, The effect of area ratio on microjet array heat transfer, Int. J. Heat Mass Transf. 54 (2011) 1782–1790, https://doi.org/10.1016/j.ijheatmasstransfer.2010.12.038.
[38] D.J. Womac, S. Ramadhyani, F.P. Incropera, Correlating equations for Impingement Cooling of Small heat Sources With Single Circular, Liquid Jets (1993).
[39] E.N. Sieder, G.E. Tate, Heat Transfer and Pressure Drop of Liquids in Tubes, Ind. Eng. Chem. 28 (1936) 1429–1435, https://doi.org/10.1021/ie50324a027.
[40] M.-Y. Wen, K.-J. Jang, An impingement cooling on a flat surface by using circular jet with longitudinal swirling strips, Int. J. Heat Mass Transf. 46 (2003) 4657–4667, https://doi.org/10.1016/S0017-9310(03)00302-8.
[41] D. Lytle, B. Webb, Air jet impingement heat transfer at low nozzle-plate spacings, Int. J. Heat Mass Transf. 37 (1994) 1687–1697, https://doi.org/10.1016/0017-9310(94)90059-0.